10.6 MICRON PARAMETRIC FREQUENCY CONVERTER

R. L. Abrams, et al

Hughes Research Laboratories

Prepared for:

Office of Naval Research
Defense Advanced Research Projects Agency

30 November 1975

10.6 MICRON PARAMETRIC FREQUENCY CONVERTER

R. L. ABRAMS, C. K. ASAWA, AND A. E. POPA

HUGHES RESEARCH LABORATORIES
3011 MALIBU CANYON ROAD
MALIBU, CALIFORNIA 90265

30 NOVEMBER 1975

SEMIANNUAL TECHNICAL REPORT 2
FOR PERIOD 1 MARCH 1975 THROUGH 31 OCTOBER 1975
CONTRACT N00014-75-C-0089

SPONSORED BY

DEFENSE ADVANCED RESEARCH PROJECTS AGENCY
ARPA ORDER NO. 1806

MONITORED BY

OFFICE OF NAVAL RESEARCH
800 NORTH QUINCY STREET
ARLINGTON, VIRGINIA 22217

UNCLASSIFIED

SECURITY CLASSIFICATION OF THIS PAGE (When Data Entered)

REPORT DOCUMENTATION PAGE		READ INSTRUCTIONS BEFORE COMPLETING FORM
1. REPORT NUMBER	2. GOVT ACCESSION NO.	3. RECIPIENT'S CATALOG NUMBER
4. TITLE (and Subtitle) 10.6 MICRON PARAMETRIC FREQUENCY CONVERTER		5. TYPE OF REPORT & PERIOD COVERED 6. PERFORMING ORG. REPORT NUMBER
7. AUTHOR(s) R. L. Abrams, C. K. Asawa, and A. E. Popa		8. CONTRACT OR GRANT NUMBER(s) N00014-75-C-0089
9. PERFORMING ORGANIZATION NAME AND ADDRESS Hughes Research Laboratories 3011 Malibu Canyon Road Malibu, California 90265		10. PROGRAM ELEMENT, PROJECT, TASK AREA & WORK UNIT NUMBERS ARPA Order No. 1806
11. CONTROLLING OFFICE NAME AND ADDRESS Defense Advanced Research Projects Agency 1400 Wilson Boulevard Arlington, Virginia 22209		12. REPORT DATE November 1975 13. NUMBER OF PAGES
14. MONITORING AGENCY NAME & ADDRESS (if different from Controlling Office) Office of Naval Research 800 No. Quincy Street Arlington, Virginia 22217		15. SECURITY CLASS. (of this report) Unclassified 15a. DECLASSIFICATION/DOWNGRADING SCHEDULE

16. DISTRIBUTION STATEMENT (of this Report)

Approved for public release: Distribution unlimited.

17. DISTRIBUTION STATEMENT (of the abstract entered in Block 20, if different from Report)

18. SUPPLEMENTARY NOTES

19. KEY WORDS (Continue on reverse side if necessary and identify by block number)

CO_2 Laser
Nonlinear Mixing
Frequency Conversion
Tunable Laser

20. ABSTRACT (Continue on reverse side if necessary and identify by block number)

This program represents an effort to demonstrate nonlinear mixing induced in a molecular gas by the application of a dc electric field. In particular, the molecule NH_2D is considered as a three-level system interacting simultaneously with applied infrared and microwave radiation. A resonant nonlinear interaction occurs resulting in the generation of a third frequency. This process is allowed because of the removal of inversion degeneracy in the gas by the applied field.

DD FORM 1 JAN 73 1473 EDITION OF 1 NOV 65 IS OBSOLETE

UNCLASSIFIED

SECURITY CLASSIFICATION OF THIS PAGE (When Data Entered)

ARPA Order No.	1806
Program Code Number	5E20
Effective Date of Contract	1 September 1974
Contract Expiration Date	31 October 1975
Amount of Contract	$99,958.00
Principal Investigator	R.L. Abrams (213) 456-6411 ext. 498
Scientific Officer	Director, Physics Program Physical Sciences Division Office of Naval Research 800 North Quincy Street Arlington, Virginia 22217

This research was supported by the Advanced Research Projects Agency of the Department of Defense and was monitored by ONR under Contract No. N00014-75-C-0089.

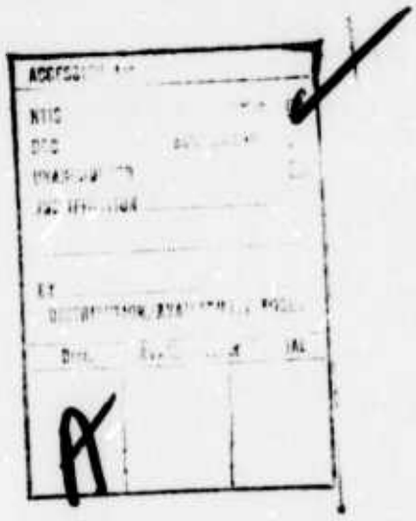

The theory of the three-level system interacting with two applied fields is treated in the general case where both doppler and collision broadening are important. It is shown that the effective resonant electro-optic coefficient for mixing of 10.6 μm radiation with 4.1 GHz microwaves in NH_2D is comparable to the value in single crystal GaAs, one of the best electro-optic materials available. The modulation process results in single sideband generation, in contrast to most modulation schemes. The dispersion in the nonlinear coefficient is also calculated. Phase mismatch during parametric interaction due to the microwave structure and its effect on parametric conversion efficiency has been considered. The decrease in the nonlinear coefficient under optical and microwave power saturation has been theoretically treated.

Significant experimental progress was made during this interim period. A new, completely enclosed, ridged waveguide Stark cell was developed. Single sideband parametric conversion at the difference frequency between the incident CO_2 laser radiation and the 4 GHz microwave radiation was accomplished with the modified cell, as predicted. This represents the first observation of resonantly-enhanced Stark-induced two-photon mixing in a gas. The parametric signal was further examined as a function of the Stark voltage, NH_2D pressure, the microwave frequency and power. The results generally confirm predictions.

TABLE OF CONTENTS

SECTION PAGE

LIST OF ILLUSTRATIONS

PREFACE

The following personnel contributed to the research reported here: Prof. Amnon Yariv, a consultant to Hughes Research Laboratories, P. Yeh, and R. L. Abrams contributed to the theoretical treatment of the nonlinear interaction. The microwave Stark cell development and optical measurements were made by A. Popa, C. K. Asawa, and T. K. Plant with the technical assistance of R. Niedziejko and R. Brower.

I. INTRODUCTION AND SUMMARY

A. Background

We anticipate that modern optical radar systems for surveillance of orbiting objects will require new types of electro-optical devices capable of frequency control and frequency conversion of infrared (IR) laser radiation. This program addresses an approach that should lead to a new class of electro-optical devices such as single sideband modulators, tunable local oscillators, and frequency shifters, using the resonant interaction of optical and microwave fields in a gas whose energy level structure is controlled by an applied electric field (Stark effect).

The molecule NH_2D has an IR absorption line that may be tuned into resonance with the P(20) 10.6 μm CO_2 laser transition by application of an electric field. This transition has been studied extensively[1,2] and has been used to intensity modulate the CO_2 laser at low frequencies.[3] More recently, at Hughes Research Laboratories, we have exploited this interaction to frequency stabilize a gigahertz tunable waveguide CO_2 laser,[4] demonstrating precise control of the waveguide laser frequency over a bandwidth greater than 1 GHz, and solving one of the major problems in CO_2 laser frequency control. The experience with these interactions in Stark tunable molecules has stimulated the concepts and ideas which are being implemented in this program.

B. Basic Concept

The energy level scheme for NH_2D is more thoroughly discussed in Section II of this report. To illustrate the basic mechanism for the interaction, consider the simplified energy level diagram shown in Fig. 1. Upon application of an electric field (of appropriate magnitude), two NH_2D energy levels, labeled 1 and 3 in Fig. 1, will become resonant with the laser frequency. A third level (level 2) is

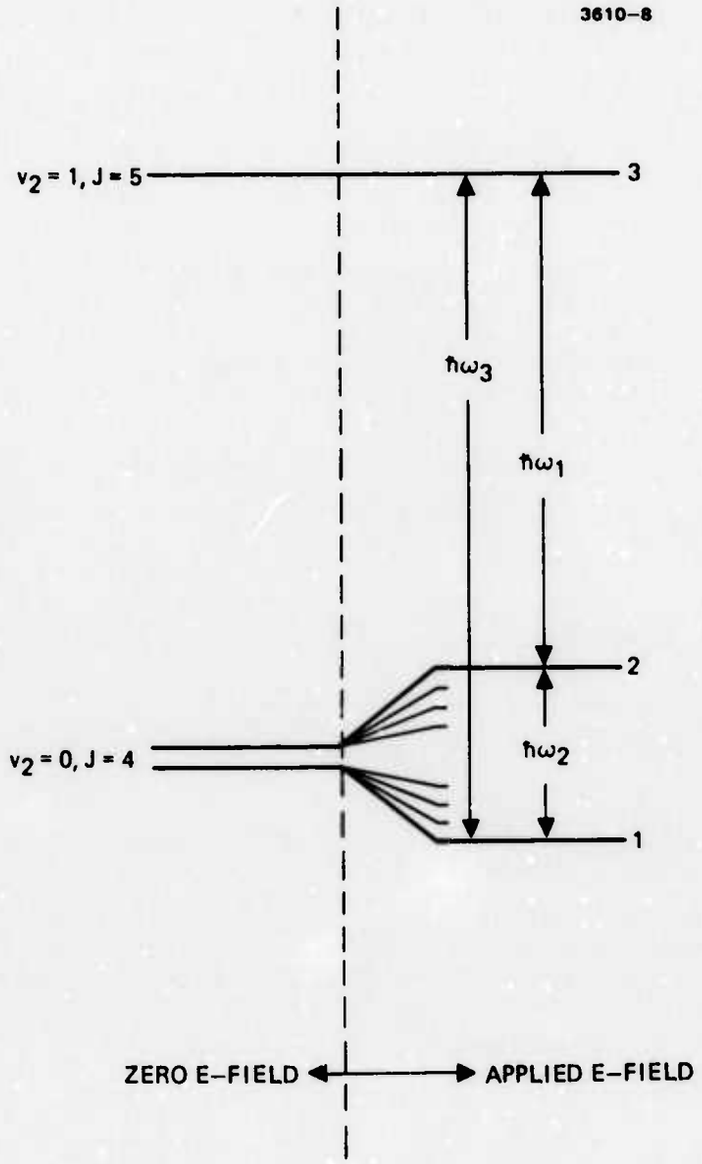

Fig. 1.
Simplified energy level diagram for NH_2D, showing relevant levels in an applied electric field. The P(20) 10.6 μm radiation is incident at frequency ω_3, ω_2 is the applied microwave frequency, and ω_1 is the newly generated sideband frequency.

also tuned by the electric field. The key element of this system is that the applied field breaks inversion symmetry and induces a permanent dipole moment. The three electric dipole moments μ_{12}, μ_{13}, μ_{23} are all nonzero, due to the applied electric field, and this allows us to consider a number of possible strong interactions which would ordinarily be weak. The proposed experiment involves the simultaneous application of two fields to the NH_2D, an applied field at ω_2 (resonant with levels 1 and 2 at ~4.1 GHz). Quantum mechanical calculations, discussed in Section II, show that it is possible to generate a signal at $\omega_1 = \omega_3 - \omega_2$, and that measurable conversion efficiency is possible with modest amounts of rf power. This surprising result is largely due to the nonvanishing dipole matrix elements induced by the applied field. In effect, the gas becomes the vehicle for a field-induced resonant nonlinear interaction.

C. Progress

Section II contains a summary of our progress on the theory of the nonlinear interaction. The resonant nonlinear coefficient is derived for stationary molecules (no doppler broadening) and the result is then integrated over the molecular velocity distribution, resulting in a general expression for arbitrary amounts of doppler and pressure broadening. The result is then extended for off-resonance operation, and it is shown that the nonlinear coefficient becomes complex, with the imaginary part displaying a magnitude considerably larger than the real part. This may be important in finding means to extend the bandwidth of the effect. The value of the coefficient is related to the high pressure limiting value of the linear absorption coefficient resulting in a simple expression for accurately estimating its magnitude. A resonant value of

$$d^{\omega_1 = \omega_3 - \omega_2} = 9.6 \times 10^{-8} \text{ esu}$$

is calculated. Phase mismatch during parametric interaction due to the microwave structure and its effect on parametric conversion efficiency has been considered; results show that considerable decrease in efficiency can occur unless the cavity is carefully designed. The decrease in the nonlinear coefficient under optical and microwave power saturation have been theoretically determined.

Significant experimental progress was made during this interim period and is summarized in Section III. The triplate microwave Stark cell was completed and tested, but excessive RFI problems were encountered. Therefore, a new, completely enclosed, ridged waveguide Stark cell was developed. The original ridged cell was designed and constructed to resonate at the theoretically specified 4.134 GHz. However, modification of the cell necessitated by high voltage breakdown, detuned the cell resonant frequency to an extent not adequately compensated for by an external stub.

Single sideband parametric conversion at the difference frequency between the incident CO_2 laser radiation and the 4 GHz microwave radiation was accomplished with the modified cell, as predicted. This represents the first observation of resonantly-enhanced Stark-induced two photon mixing in a gas. The experiment was performed by spectrally resolving the parametric signal from the CO_2 carrier signal in order to distinguish the newly generated parametric signal from the modulated carrier signal. The parametric signal was further examined as a function of the Stark voltage, NH_2D pressure, the microwave frequency and power. The results generally confirm predictions. These experiments showed that the modifications to the Stark cell and inadequate microwave coupling to the cell resulted in frequency pulling of the maximum parametric signal, no observation of microwave power saturation, and lowered the observed conversion efficiency from the expected 10^{-2} to 10^{-3}.

D. Plans

During the next half of the program the emphasis will be directed toward four areas: (1) further development of an efficient microwave

Stark cell cavity, (2) further detailed analysis of the parametric data on NH_2D obtained during the first half of this program, (3) examination of parametric interaction with other CO_2 carrier lines, and (4) search for other nonlinear gaseous systems. A tunable waveguide CO_2 laser will be utilized to peak the optical resonance in order to enhance parametric conversion at the double resonance point. Based on the results of these efforts, a single sideband modulator with 10% conversion efficiency will be fabricated and demonstrated.

II. THEORY

A. Introduction

This section contains a summary of our present theoretical understanding of nonlinear frequency mixing in a three-level system. The analysis originally presented in our technical proposal is repeated here for completeness. In addition, we have performed a detailed analysis of the pressure dependence of the nonlinear coefficient, as well as a treatment of the frequency dependence of the interaction and saturation effects. These results will be useful for extension of the operating bandwidth of the parametric frequency converter.

Nonlinear optical mixing phenomena such as parametric oscillation, frequency up-conversion and the electro-optic (Pockels) effect require that the atomic system lack an inversion symmetry. Liquids and gases, by virtue of their random orientation, possess a macroscopic inversion symmetry and hence have not been deemed appropriate for nonlinear and modulation applications. In principle, the symmetry is broken when a dc electric field is present, so that a gas or a liquid in an electric field may be expected to display nonlinear optical properties.

To estimate the dc-induced optical nonlinearity in a gas, we carry out a quantum mechanical analysis. The analytic results are then applied to calculate the nonlinear optical constants of NH_2D, which are especially suitable for this application.

The nonlinear optical coefficients are used in an electromagnetic analysis to calculate the down-conversion efficiency of the output of the P(20) CO_2 laser line $\omega_o = 944\ cm^{-1}$ to $\omega_o - \Delta$ by mixing with a microwave field frequency at $\Delta = 4134$ MHz.

B. Quantum Mechanical Derivation of the Nonlinear Optical Mixing Terms

The model assumes a three-level atomic system as shown in Fig. 2. Oscillating fields at ω_2 (microwave) and ω_3 are applied and a solution is sought for the polarization component at $\omega_1 = \omega_3 - \omega_2$.

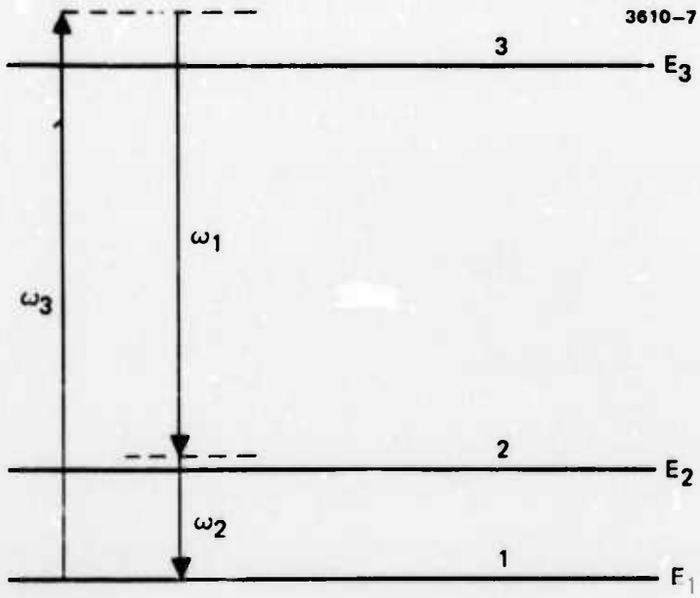

Fig. 2. Three-level system used in deriving the nonlinear optical coefficient.

We apply the density matrix formalism. The component of the polarization is given by

$$P_\alpha = N\mathrm{tr}\,(\rho\mu_\alpha) \tag{1}$$

where N is the density of molecules, ρ the density matrix, and $\vec{\mu}$ the dipole moment operator. The term tr stands for the trace (sum of diagonal terms).

The system Hamiltonian is taken as

$$= H_o + V = H_o - \vec{\mu}\cdot\vec{E}(t)\,, \tag{2}$$

where $\vec{E}(t)$ is the applied oscillating electric field. The effect of the dc field is lumped into the unperturbed Hamiltonian H_o. The density matrix ρ can be expanded in powers of V as

$$\rho = \rho^{(0)} + \rho^{(1)} + \rho^{(2)} + \ldots \tag{3}$$

where $\rho^{(n)} \propto V^n$. Thus $\rho^{(0)}$ is the thermal equilibrium value of ρ.

$$\rho^{(0)} = \bar{\rho} = \frac{\exp\left(-\frac{H_o}{kT}\right)}{\mathrm{tr}\left[\exp\left(-\frac{H_o}{kT}\right)\right]}\,. \tag{4}$$

In the absence of any relaxation phenomena, ρ obeys

$$\frac{\partial\rho_{ij}}{\partial t} = -i\omega_{ij}\,\rho_{ij} - \frac{i}{\hbar}\,[V,\rho]_{ij} \tag{5}$$

where $\hbar\omega_{ij} = E_i - E_j$. To include the effect of collisions we modify (5) phenomenologically to

$$\frac{\partial \rho_{ij}}{\partial t} = - i\omega_{ij} \rho_{ij} - \frac{i}{\hbar} [V, \rho]_{ij} - \gamma_{ij}(\rho - \bar{\rho})_{ij} \tag{6}$$

so that γ_{ij} $(i \neq j)$ is the rate for phase destroying collisions caused by elastic and inelastic collisions. γ_{ii} is the inverse of the lifetime of level i.

By using (3) in (6) we obtain

$$\frac{\partial \rho_{ij}^{(n)}}{\partial t} = - (i\omega_{ij} + \gamma_{ij}) \rho_{ij}^{(n)} - \frac{i}{\hbar} [V, \rho^{(n-1)}]_{ij} ,$$

whose formal solution is

$$\rho_{ij}^{(n)}(t) = - \frac{i}{\hbar} \int_{-\infty}^{t} dt' e^{i(\omega_{ij} - i\gamma_{ij})(t'-t)} [V(t'), \rho^{(n-1)}(t')]_{ij} \tag{7}$$

We solve (7) for the case when

$$\bar{E}(t) = \frac{\overline{E_3}}{2} e^{i\omega_3 t} + \frac{\overline{E_2}}{2} e^{i\omega_2 t} + c.c. \tag{8}$$

The desired mixing term at $\omega_1 = \omega_3 - \omega_2$ results in lowest order from $\rho^{(2)}$ in (1); i.e.,

$$P^{(2)} = N \mathrm{tr} [\rho^{(2)} \mu_\alpha] \tag{9}$$

so that two iterations of (7) are necessary.

Anticipating the result, we keep only resonant terms (i.e., those with nearly vanishing denominators) and take $\bar{\rho}_{33} = 0$ obtaining

$$\rho_{13}^{(1)} = -\frac{i}{2\hbar} \frac{\bar{\rho}_{11}\mu_{13}E_3}{[i(\omega_{31} - \omega_3) - \gamma_{13}]} e^{i\omega_3 t}$$

$$\rho_{12}^{(1)} = \frac{i}{2\hbar} \frac{(\bar{\rho}_{22} - \bar{\rho}_{11})\mu_{12}E_2}{[i(\omega_{21} - \omega_2) - \gamma_{12}]} e^{i\omega_2 t}$$

which are used in (7) and (9) to give

$$P_\alpha^{(2)} = \rho_{23}^{(2)} (\mu_\alpha)_{32} + \rho_{32}^{(2)} (\mu_\alpha)_{23}$$

$$= \frac{1}{4\hbar^2} \left\{ \frac{N_1\mu_{12}\mu_{13}(\mu_\alpha)_{32}}{[\gamma_{13} + i(\omega_3 - \omega_{31})][\gamma_{32} - i(\omega_{32} - \omega_1)]} \right.$$

$$\left. - \frac{(N_2 - N_1)\mu_{12}\mu_{13}(\mu_\alpha)_{32}}{[\gamma_{12} - i(\omega_2 - \omega_{21})][\gamma_{32} - i(\omega_{32} - \omega_1)]} \right\} E_3 E_2^* e^{i\omega_1 t}$$

$$+ \text{c.c.} \qquad (10)$$

In the language of nonlinear optics[5] we characterize the optical mixing by a parameter

$$d_{\alpha 32}^{\omega_1 = \omega_3 - \omega_2},$$

defined by

$$P_\alpha^{\omega_1 = \omega_3 - \omega_2} = \frac{1}{2} d_{\alpha 32}^{\omega_1 = \omega_3 - \omega_2} E_3 E_2^* e^{i(\omega_3 - \omega_2)t}$$

$$+ \text{complex conj}, \qquad (11)$$

so that from (10)

$$d_{\alpha 32}^{\omega_1 = \omega_3 - \omega_2} = \frac{1}{2\hbar^2} \left[\frac{N_1 \mu_{12} \mu_{13} (\mu_\alpha)_{32}}{[\gamma_{13} + i(\omega_3 - \omega_{31})][\gamma_{32} - i(\omega_{32} - \omega_1)]} \right.$$

$$\left. - \frac{(N_2 - N_1) \mu_{12} \mu_{13} (\mu_\alpha)_{32}}{[\gamma_{12} - i(\omega_2 - \omega_{21})][\gamma_{32} - i(\omega_{32} - \omega_1)]} \right]. \qquad (12)$$

This is our basic result, valid for a homogeneously broadened transition. In the following section we will integrate it over the doppler distribution to derive the nonlinear coefficients for a gas exhibiting simultaneous pressure and doppler broadening.

C. Pressure Dependence and Dispersion

The expression for $d^{\omega_1 = \omega_3 - \omega_2}$ given above assumed operation in the pressure broadened region where doppler broadening is negligible. For optimization of the nonlinear coefficient it will be important to understand in detail the transition region and the pressure dependence of both the absorption (γ) and the nonlinear coefficients. The behavior of d and γ (in this region) as well as their dispersion, are also of fundamental spectroscopic importance and contain useful information about the broadening and collision mechanism.

We now allow for a velocity distribution of the gas molecules described by a Maxwellian

$$g(v) = \frac{1}{\sqrt{2\pi}\sigma} e^{-v^2/2\sigma^2} \tag{13}$$

so that σ is the rms velocity. Assuming perfect resonance $\omega_{31} = \omega_3$ and $\omega_{32} = \omega_1$ for stationary molecules and taking $N_1 = N_2$, $N_3 = 0$ we replace $(\omega_{32} - \omega_1)$ in (12) by $\omega_{32} v/c$ to allow for the doppler energy shift of atoms v. Similarly, $(\omega_3 - \omega_{31}) \rightarrow -\omega_{31} v/c$. The velocity averaged $d^{\omega_1 = \omega_3 - \omega_2}$ is thus

$$d^{\omega_1 = \omega_3 - \omega_2} = -\frac{N_1 \mu_{12} \mu_{13} \mu_{32}}{2\hbar^2} \int \frac{g(v)}{\left(\frac{\omega_{32} v}{c} - i\Gamma\right)\left(\frac{\omega_{31} v}{c} - i\Gamma\right)} dv \tag{14}$$

where $\Gamma \equiv \gamma_{13} = \gamma_{32}$ is the sum of the natural and pressure induced linewidths.

The integral occurring in (14) can be separated into sums of plasma dispersion integrals and is evaluated to be

$$\int dv = \sqrt{\frac{\pi}{2}} \frac{c}{\gamma\Gamma\omega_{21}} \left\{ F\left(\frac{c}{\sqrt{2}\,\sigma\omega_{32}}\right) - F\left(\frac{c}{\sqrt{2}\,\sigma\omega_{31}}\right) \right\} \tag{15}$$

$$\simeq \sqrt{\frac{\pi}{2}} \frac{c}{\sigma\omega_{31}} \frac{\partial F}{\partial \Gamma} \quad \text{for} \quad \omega_{21} \ll \omega_{31}, \omega_{32}, \tag{16}$$

where

$\int dv$ refers to the integral in (14) and

$F(x) = e^{x^2} \operatorname{erfc}(x)$

(erfc(x) = complementary error function).

Using (16) in (14) yields

$$d^{\omega_1 = \omega_3 - \omega_2} = - \frac{N_1 \mu_{12} \mu_{13} \mu_{32}}{2\hbar^2} \sqrt{\frac{\pi}{2}} \frac{c}{\sigma \omega_{31}} \left(\frac{\partial F}{\partial \Gamma} \right) . \qquad (17)$$

We note that the argument of the F function, $c\Gamma/(\sqrt{2}\,\sigma\omega_{31})$, is the ratio of the homogeneous linewidth to the doppler linewidth. It is essentially proportional to pressure so that eq. (17) describes the pressure dependence of the nonlinear coefficient d.

Although a numerical estimate of d based on (17) is possible, a safer procedure and one that serves as a check is to relate d to the linear absorption coefficient (due to $1 \rightarrow 3$ transitions) γ. Using the same formalism and symbols we obtain

$$\gamma = \frac{4\pi |\mu_{13}|^2 N_1}{\sigma \hbar} \sqrt{\frac{\pi}{2}} \; F\left(\frac{c\Gamma}{\sqrt{2}\,\sigma\omega_{31}} \right)$$

$$\equiv \gamma_H \sqrt{\pi} x e^{x^2} \operatorname{erfc}(x) .$$

$$x = \left(\frac{c\Gamma}{\sqrt{2}\,\sigma\omega_{31}} \right) \qquad (18)$$

so γ_H = value of γ at $x \rightarrow \infty$ (high pressure). Combining (18) with (17) yields, after some mathematical manipulation,

$$d^{\omega_1 = \omega_3 - \omega_2} = - \frac{c\,\mu_{12}}{8\pi\hbar\omega_{31}} \left(\frac{\mu_{23}}{\mu_{13}} \right) \sqrt{\frac{\pi}{2}} \frac{c\,\partial_H}{\sigma\omega_{31}} \left[2x^2 F(x) - \frac{2}{\sqrt{\pi}}\, x \right] . \qquad (19)$$

Note that μ_{12} is determined precisely from the Stark splitting rate ($\Delta E_{Stark} = 2\mu_{12}E$ at high fields) $\mu_{23}/\mu_{31} \sim 1$, while γ_H is the asymptotic value of the absorption coefficient of the $1 \rightarrow 3$ transition at high pressures ($x >> 1$).

D. Nonlinear Coefficient of NH_2D

From (12) it follows that a large nonlinear coefficient

$$d_{\omega 32}^{\omega_1 = \omega_3 - \omega_2}$$

results when the applied photon energies of the microwave field ω_2 and the optical frequency ω_3 are nearly resonant with some transitions ω_{31} and ω_{32}.

An atomic system which meets these requirements is that of the molecule NH_2D. The relevant transitions are rotational vibrational and are shown in Fig. 3.

Levels 1 and 2 are nearly degenerate with a (zero field) splitting of 644 MHz. Their (ν_2) vibrational symmetry is indicated on the left. Level 1 is odd; level 2 is even. The application of a dc electric field causes a quasilinear Stark splitting of these two states as shown. At a field of 3570 V/cm the transition energy $\hbar\omega_{31}$ is equal to the photon energy of the P(20) CO_2 laser line at 944 cm^{-1}. At this field the $|M| = 4$ states separation is 4134 MHz (Ref. 6).

The splitting $\hbar\omega_{21}$ is given by

$$\hbar\omega_{21} = 2\sqrt{\Delta^2 + \mu_{ab}^2 E^2} \qquad (20)$$

where μ_{ab}, the dipole matrix element connecting level 1 and 2, is accurately determined from Stark effect measurements[6] to be $\mu_{ab} = 1.14 \times 10^{-18}$ esu.

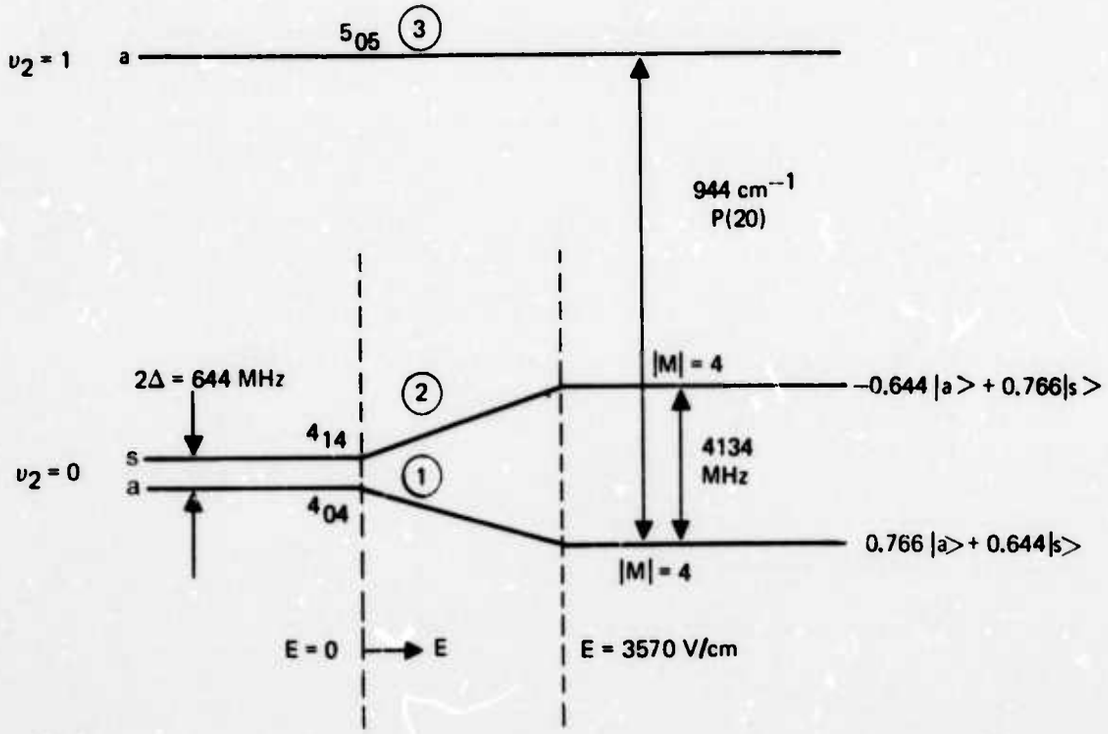

Fig. 3. Some of the energy levels relevant to the derivation of the nonlinear coefficient d_{123} (a is antisymmetric, s is symmetric).

The applied dc field causes an admixture of states 1 and 2. This admixture is crucial. Without it the dipole matrix element $\langle 1|\mu|3\rangle = \langle a|\mu|a\rangle = 0$ by symmetry. It follows from (12) that the nonlinear coefficient is zero. In the presence of a field the vibrational symmetry is destroyed and

$$|2\rangle = -a_1|a\rangle + a_2|s\rangle$$

$$|1\rangle = a_2|a\rangle + a_1|s\rangle \tag{21}$$

where

$$\frac{a_2}{a_1} = \frac{\Delta}{\mu_{ab}E} + \sqrt{1 + \frac{\Delta^2}{\mu_{ab}^2 E^2}} \tag{22}$$

It follows that the dipole matrix element μ_{12} which enters into the expression (12) for d is

$$\mu_{12} = \left(a_2^2 - a_1^2\right)\mu_{ab} . \tag{23}$$

At an applied field of 3570 V/cm, needed to resonate the P(20) CO_2 laser line, we have from (15)

$$|2\rangle = -0.644|a\rangle + 0.766|s\rangle$$

$$|1\rangle = 0.766|a\rangle + 0.644|s\rangle \tag{24}$$

and

$$\mu_{12} = \mu_{ab}(0.586 - 0.414)$$

$$= 0.174\mu_{ab} = 0.198 \times 10^{-18} \text{ esu} \tag{25}$$

Equation 19 relates the nonlinear coefficient to the experimentally measured[3] high pressure value of the linear absorption coefficient. Although it is possible to relate the nonlinear coefficient directly to the dipole matrix elements (see eq. 17), the uncertainties in estimating the percent concentration of NH_2D in the mixture as well as the partition function for level 1 are such that it is more reasonable to use the measured absorption directly. In this way, the NH_2D concentration and partition function are automatically included. From the data of Ref. 3, we estimate for a 50:50 ND_3 - NH_3 mixture,

$$\gamma_H = 0.042 \text{ cm}^{-1} \tag{26}$$

$$\Gamma/P = 2\pi(32 \text{ MHz/Torr}) \tag{27}$$

Inserting $\sigma = \sqrt{RT/m}$, μ_{12}, and the laser frequency ω_{31} into eq. 19, we have

$$d^{\omega_1 = \omega_3 - \omega_2} = 8.27 \times 10^{-6} \gamma_H G(x)$$

$$= 3.47 \times 10^{-7} G(x) \text{ esu} \tag{29}$$

where γ_H is in cm^{-1}, and G(x) is dimensionless, defined as

$$G(x) = 2x \left[\frac{1}{\sqrt{\pi}} - x e^{x^2} \text{erfc}(x) \right] \tag{30}$$

$$x = \frac{c\Gamma}{\sqrt{2}\,\sigma\omega_{31}} = \frac{\text{Pressure Broadened Linewidth}}{\text{Doppler Linewidth}} \tag{31}$$

The function G(x) versus x, and equivalently d versus pressure for NH_2D, are shown in Fig. 4. The peak value for the nonlinear coefficient occurs at ~1.2 Torr and has a value

$$d^{\omega_1 = \omega_3 - \omega_2} = 9.6 \times 10^{-8} \text{ esu} . \tag{32}$$

The coefficient d estimated above refers to the generation of a sideband at ω_1 by mixing a CO_2 P(20) line with a microwave field ω_2 (at 4134 MHz). It is appropriate to compare it with the electro-optic coefficient r_{14} of GaAs which can be used, alternatively, to generate the sideband by conventional electro-optic modulation.

Using the correspondence[7]

$$r_{j\ell k} = - \frac{2\epsilon_o}{\epsilon_j \epsilon_\ell} d_{jk\ell} \tag{33}$$

we have

$$\frac{(n^3 r)_{NH_2D}}{(n^3 r)_{GaAs}} \sim 1.1 . \tag{34}$$

We reach the conclusion that as far as sideband generation, dc biased NH_2D is comparable to GaAs (which is one of the best infrared modulation materials). We must recognize, however, that this large coefficient was obtained by exploiting the resonant nature of the effect. The penalty we pay is that of reduced bandwidth In the following section, we consider the frequency response of the nonlinear coefficient.

E. Dispersion of the Nonlinear Coefficients

The treatment up to this point assumed that the applied frequencies ω_3 and ω_2 were exactly equal to the center frequencies of the

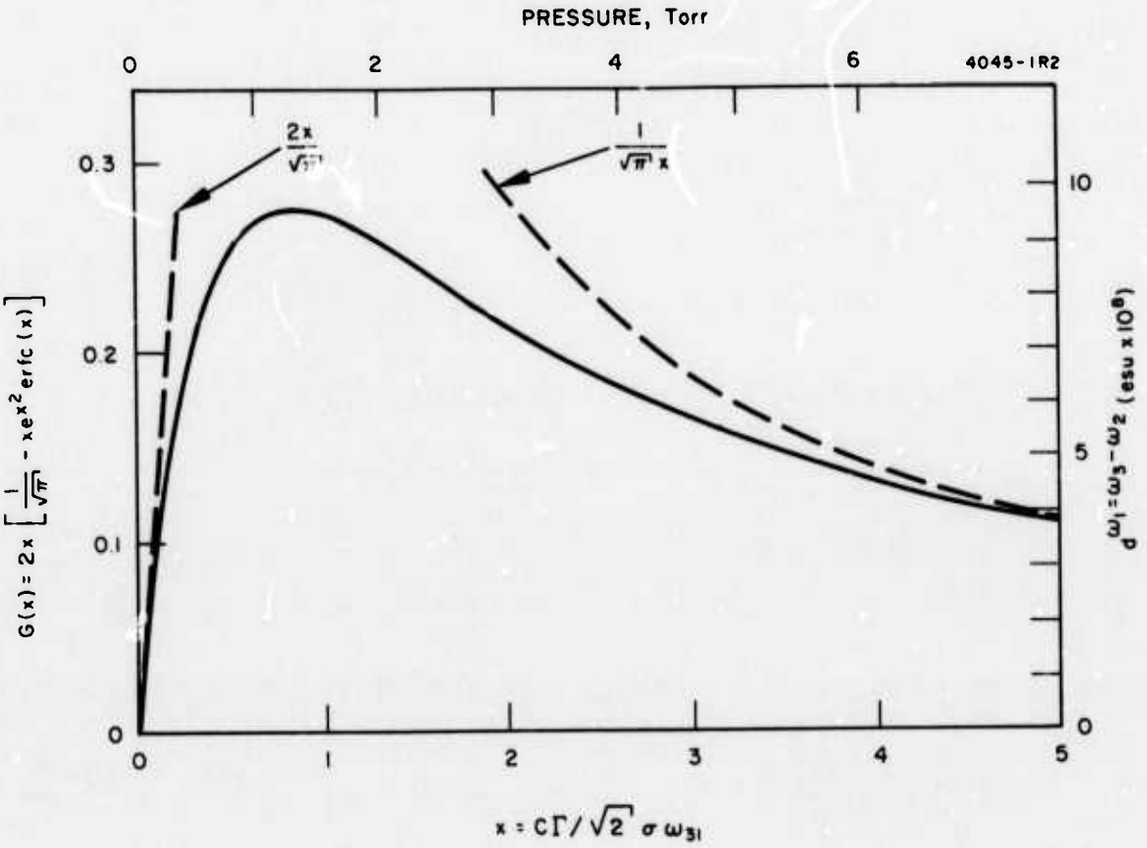

Fig. 4. Dependence of NH_2D nonlinear coefficient on pressure for exact resonance. Equivalently, the functional form of G(x) is shown.

respective transitions. This results, as shown above, in real nonlinear coefficients, d. If one allows a frequency deviation $\omega_3 - \omega_{31} \neq 0$, d is complex. The analysis is involved and will be reported in full in the final report. The imaginary part of d is only slightly smaller than the real part of d. Plots of both the imaginary and real part of d are shown in Fig. 5 as a function of the frequency deviations for three different pressures.

F. Frequency Conversion Efficiency and Phase Mismatch in the Microwave Structure

One important class of applications of the dc-induced optical nonlinearity is that of parametrically converting from ω_3, which is our case corresponds to the P(20) CO_2 laser line, to $\omega_1 = \omega_3 - \omega_2$ where ω_2 is the microwave frequency at 4134 MHz. The construction of a practical microwave cavity for parametric conversion requires the consideration of conversion efficiency and phase mismatches, since phase velocities in microwave structures may be considerably different from free space phase velocities. Here we estimate the conversion efficiency for expected realizable conditions.

The parametric signal conversion efficiency from the CO_2 carrier power to the parametric signal power is determined from the solution of the coupled equations.[7]

$$\frac{dA_1}{dx} = -i\frac{g}{2}A_3 e^{-i\Delta kx}$$

$$\frac{dA_3}{dx} = -\frac{\alpha_3}{2} - i\frac{g}{2}A_1 e^{i\Delta kx} \qquad (35)$$

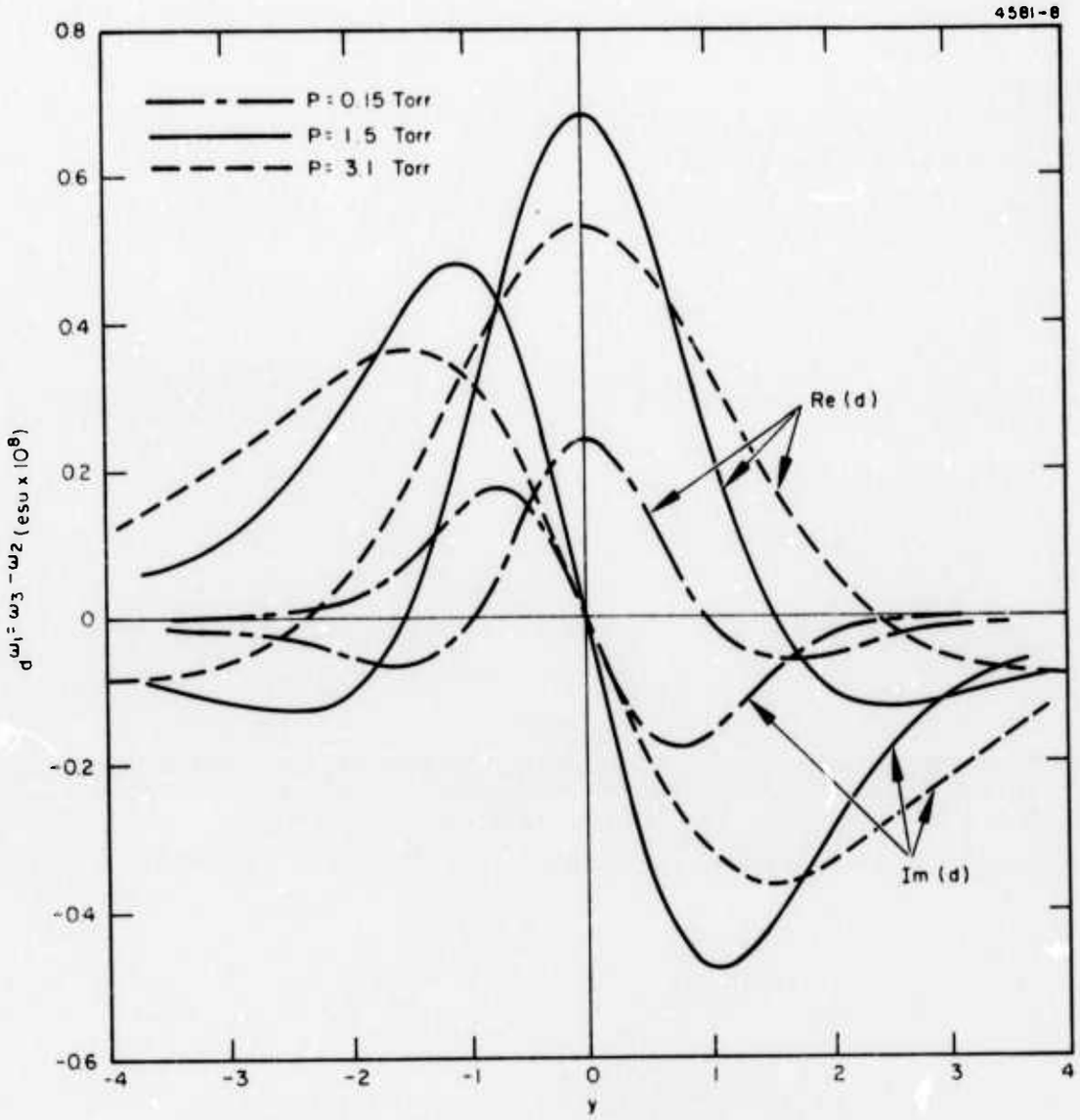

Fig. 5. Dependence of the real and imaginary parts of the nonlinear coefficient on detuning parameter

$$y = \frac{C(\omega_3 - \omega_{31})}{\sqrt{2}\,\sigma\,\omega_{31}} \quad .$$

It is assumed that $\omega_2 - \omega_{21} = 0$.

where

$$A_i = \sqrt{\frac{n_i}{\omega_i}}\, E_i$$

$$g = \sqrt{\frac{\mu_o}{\epsilon_o}\,\frac{\omega_1\omega_3}{n_1 n_3}}\, d_{yyz}^{\omega_1 = \omega_3 - \omega_2} E_2 ,$$

$\Delta k = k_3 - (k_1 + k_2)$, the phase mismatch, (36)

α_3 = the absorption coefficient for the A_3 field.

The effect of absorption for $\alpha_3 \sim 0.01\ cm^{-1}$ is small. Setting $\alpha_3 = 0$, the solutions for $A_1(x)$ and $A_3(x)$ are readily obtained from (35). The conversion efficiency η from the CO_2 A_3 field to the parametric A_1 field is their given by

$$\eta \equiv \left|\frac{A_1(x)}{A_3(o)}\right|^2 = \frac{g^2}{(\Delta k)^2 + g^2}\, \sin^2\left(\frac{\sqrt{(\Delta k)^2 + g^2}}{2}\, x\right), \qquad (37)$$

where

x = parametric interaction distance in cm

$A_3(o)$ is proportional to the CO_2 carrier electric field at the beginning of the interaction

$A_1(x)$ is proportional to the parametric signal electric field at distance x

g = gain coefficient in cm^{-1}

Δk = phase mismatch in cm^{-1}.

When $\Delta k = 0$, the efficiency is

$$\eta = \sin^2 \left(\frac{g}{2} x\right) . \tag{38}$$

To estimate g we use the following set of conditions:

$$E_2 \sim 4 \times 10^4 \ \frac{V}{m} . \tag{39}$$

This value is based on a microwave cavity design with a Q of 100 and an input power $P_2 = 1$ W.

$$d_{yyz} = 3.55 \times 10^{-22} \text{ MKS}$$

$$\omega_3 = 1.779 \times 10^{14} \ (= 944 \text{ cm}^{-1}) \tag{40}$$

The result is

$$g = 0.01 \text{ cm}^{-1} . \tag{41}$$

With $\Delta k = 0$ and $g = 0.01$ cm^{-1}, complete conversion ($\eta = 1$) is attainable in an interaction distance π/g or 314 cm as determined from (38).

If $\Delta k \neq 0$, however, unity efficiency cannot be attained. The maximum efficiency occurs for an interaction distance

$$x = \frac{\pi}{\sqrt{(\Delta k)^2 + g^2}} \tag{42}$$

with a maximum of

$$\frac{g^2}{(\Delta k)^2 + g^2} \tag{43}$$

The conversion efficiency versus x for $g = 0.01\ cm^{-1}$ and $\Delta k = 0, 0.03, 0.06$, and $0.10\ cm^{-1}$ are shown in Fig. 6. Significant decrease of efficiency with increasing phase mismatch can be expected.

Phase mismatch may arise from a waveguide structure. The propagation vector k of free space, which perfectly matches the carrier and parametric signal momentum vectors, is resolved into transverse cutoff wave vector $\vec{k}_c$ and the longitudinal waveguide vector $\vec{k}_g$ inside the waveguide,

$$\vec{k} = \vec{k}_c + \vec{k}_g \ . \tag{44}$$

The optical propagation vectors must match the guide wave vector for optical propagation along the guide for efficient conversion. Since $|k_g|$ is smaller than $|k|$, a mismatch Δk occurs. The mismatch Δk can be determined from

$$\lambda_g = \frac{\lambda}{\sqrt{1 - \left(\frac{\lambda}{\lambda_c}\right)^2}} \tag{45}$$

where λ_g is the guide wavelength, λ is the free space wavelength, and λ_c is the cutoff wavelength for the transverse wave.

It is clear that in the design of a cavity, λ_c should be made considerably larger than the free space wavelength λ to reduce Δk. As previously noted, λ_c for a ridged waveguide is several times larger than the cutoff wavelength for a rectangular waveguide of equivalent dimensions and thus the ridged waveguide cavity appeared to be appropriate for this program. Increasing λ_c further will require

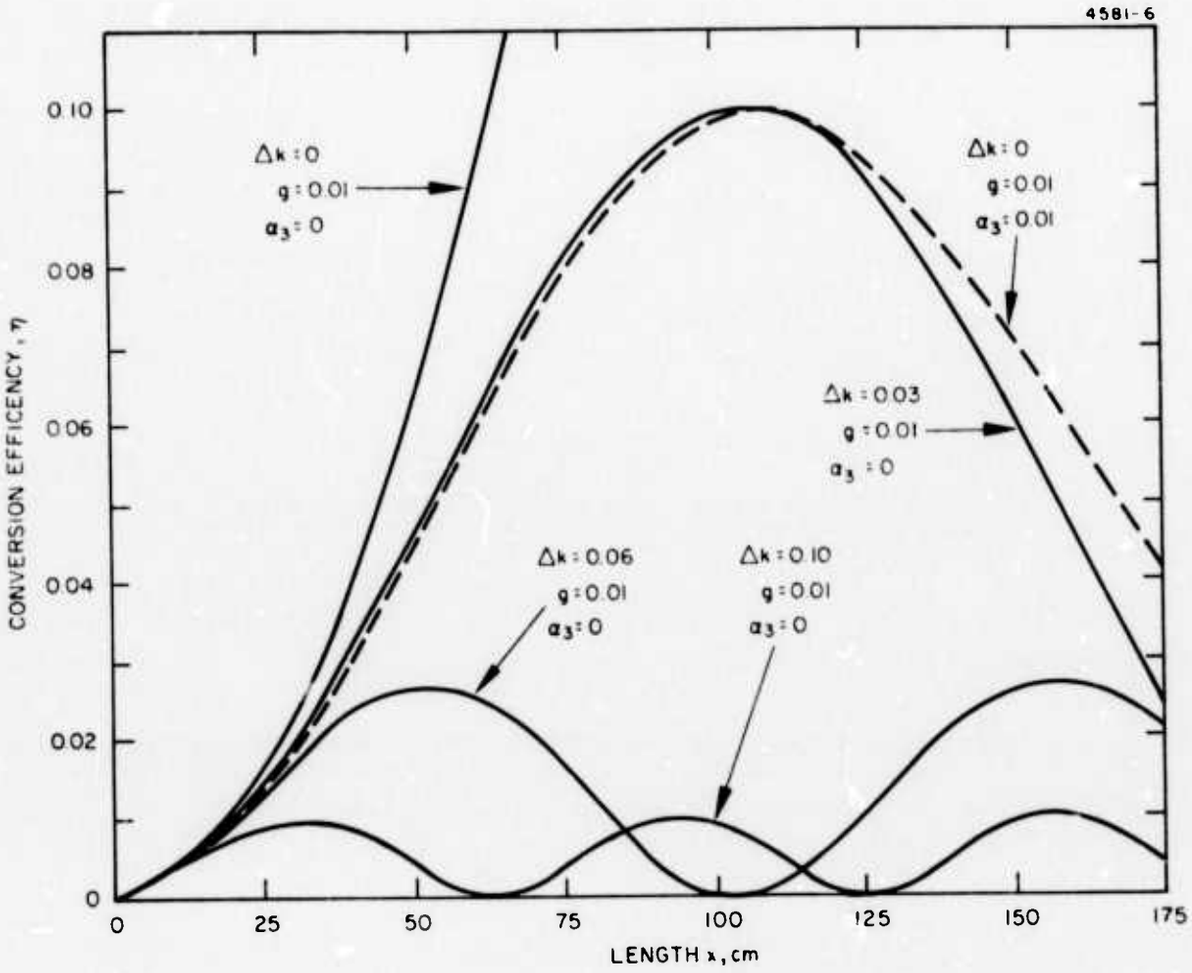

Fig. 6. Conversion efficiency versus interaction distance for several values of Δk, g, α_3.

increase of lateral dimensions and the distribution of microwave energy over a large volume. These considerations will be investigated during the next period.

Another possible method for reducing Δk to zero is to waveguide the CO_2 beam in the direction of the $\vec{k}$ vector. For the present cavity, the direction of the optical beam would have to be 27^o from the guide axis. Phase changes on reflection may be a problem. This possibility will also be further examined.

The conversion efficiency for finite absorption α_3 of the carrier by the NH_2D cell can be readily calculated. Solving for the case where $\Delta k^2 + g^2 >> \alpha_3/2$, an expression is obtained for η. A curve for the parametric values $\Delta k = 0.03$, $g = 0.01$, and $\alpha_3 = 0.01$ is graphed in Fig. 6: for these values and for x small, the effect of the absorption of the carrier is small, as expected.

G. Saturation Effects

For reasons similar to the onset of saturation in linear absorption or amplification, we expect the nonlinear coefficient given by (17) to decrease as the intensity ω_3 (the P(20) line) or at ω_2 increases. Let us consider the saturation by the ω_3 field first. There are two physical mechanisms through which saturation sets in: (1) a reduction in the population difference $N_1 - N_3$ caused by induced transitions from $1 \rightarrow 3$, and (2) power broadening of the effective linewidth which (see eq. (17)) reduces d. The presence of a field at E_2 gives rise to similar results, but since $N_1 \approx N_2$ in our case, only the power broadening is operative.

To obtain the saturation corrections, we continue the perturbation solution (10) to fourth order in V. We solve specifically for terms in which

$$P_1^{(4)\omega_1=\omega_3-\omega_2} \propto E_3 E_2^* (E_2 E_2^*) e^{i(\omega_3-\omega_2)t} \tag{46}$$

and

$$P_2^{(4)\omega_1=\omega_3-\omega_2} \propto E_3 E_2^* (E_3 E_3^*)\, e^{i(\omega_3-\omega_2)t} \tag{47}$$

The first term will describe microwave (ω_2) saturation while the second one gives the saturation due to the laser field at ω_3.

The exact solution for (46) and (47) is tedious but straightforward. The total polarization at $\omega_1 = \omega_3 - \omega_2$ is obtained by adding (46) and (47) to (10). If we factor out the common $E_3 E_2^*$ factor we can express the effect of saturation by modifying (12) to

$$d_{\alpha 32}^{\omega_1=\omega_3-\omega_2} = \frac{N_1 \mu_{12} \mu_{13} (\mu_o)_{32}}{2\hbar^2 \gamma_2^2} \left[1 - \frac{|(\bar{\mu} \cdot \bar{E}_3)_{31}|^2}{4\hbar^2 \gamma_2^2} - \frac{6|(\bar{\mu} \cdot E_3)_{31}|^2}{4\hbar^2 \gamma_2 \gamma_1} \right.$$

$$\left. - \frac{|(\bar{\mu} \cdot \bar{E}_2)_{21}|^2}{4\hbar^2 \gamma_2^2} \right] \tag{48}$$

where

$$\gamma_2 \equiv \gamma_{13} \approx \gamma_{23} \text{ and } \gamma_1 \equiv \gamma_{11} \approx \gamma_{22} \approx \gamma_{33}.$$

The second term in the square brackets describes saturation due to power broadening of levels 1 and 3. The third term describes saturation due to reduction of $N_1 - N_3$ and the last term reflects power broadening due to induced $2 \longleftrightarrow 1$ transitions by E_2.

1. Estimate of Saturation Intensities

a. Laser Field Saturation – Assume $\gamma_1 \approx \gamma_2$. The reduction in d is significant when

$$|(\bar{\mu} \cdot \bar{E}_3)_{31}|^2 \geq \frac{4\hbar^2\gamma_2^2}{\left(1 + \frac{6\gamma_2}{\gamma_1}\right)}$$

Using

$$\frac{\gamma_2}{2\pi} \approx 32 \text{ MHz/Torr (i.e., } \gamma_2 = 2 \times 10^8 \, P_{\text{Torr}})$$

$$\mu_{13} = 0.33 \times 10^{19} \text{ esu} = 0.11 \times 10^{-30} \text{ MKS}$$

$$I_3 = \frac{c\epsilon_o E_3^2}{2}$$

$$P = 1 \text{ Torr}$$

$$(I_3)_{sat} = \frac{2\hbar^2\gamma^2 c\epsilon_o}{\mu_{13}^2\left(1 + \frac{6\gamma_2}{\gamma_1}\right)}$$

$$= \frac{2 \times (1.054 \times 10^{-34})^2 \times (2 \times 10^8)^2 \times 3 \times 10^8 \times 10^{-9}}{\left(1 + \frac{6\gamma_2}{\gamma_1}\right)(0.11 \times 10^{30})^2 \, 36\pi}$$

$$= \frac{1.94\gamma \times 10^4}{\left(1 + \frac{6\gamma_2}{\gamma_1}\right)} \quad \frac{\text{watts}}{\text{cm}^2} \, .$$

The saturation intensity depends on γ_2/γ_1, i.e., the ratio of the phase collision rate (γ_2) to the population relaxation rate (γ_1). This ratio is to be considered as a parameter to be determined.

The experimental data of Thielman and Davis[8] extrapolated to P = 1 Torr yields $(I_3)_{sat}$ = 347 watts/cm^2. By equating this number to

$$\frac{2 \times 10^4}{1 + \frac{6\gamma_2}{\gamma_1}}$$

we obtain $\gamma_2/\gamma_1 = 9.61$.

2. Microwave Saturation

From the last term in (48) we define the saturation field E_{2s} as that satisfying

$$E_{2s}^2 = \frac{4h^2\gamma_2^2}{\mu_{12}^2}.$$

Use

$$\gamma_2 = 2 \times 10^8 \, P(\text{Torr})$$

$$\mu_{12} = 0.198 \times 10^{-18} \text{ esu} = 0.66 \times 10^{-30} \text{ MKS}$$

$$E_{2s}^2 = 3.7 \times 10^9 \, (\text{Volt/m})^2$$

$$P = 1 \text{ Torr.}$$

The corresponding input power to the microwave cavity depends on the cavity "Q" and its configuration. The power corresponding to $E_{2s}^2 = 3.7 \times 10^9 \, (\text{Volt/m})^2$ is ~2.3 W.

III. EXPERIMENTAL PROGRESS

A. Introduction

Significant experimental progress was made during this interim period. We developed a new microwave "ridged-waveguide" NH_2D Stark cell cavity. Single sideband parametric conversion at the difference frequency between the incident CO_2 laser radiation and the 4 GHz microwave radiation was accomplished with the cell as predicted. This represents the first observation of parametric conversion in a gaseous Stark cell. We performed the experiment by spectrally resolving the parametric signal from the CO_2 carrier signal in order to distinguish the newly generated parametric signal from any modulated carrier signal.

The parametric signal was further examined as a function of the Stark voltage, the Stark cell NH_2D pressure, the microwave frequency and power. The results generally confirm predictions. However, the measurements have shown that optimum experimental conditions were not precisely met. The parametric output versus Stark voltage for several microwave frequencies and versus microwave power clearly indicates that the interaction occurred with the microwave cavity nonoptimally coupled so that maximum double-resonance enhancement did not occur. In these experiments the maximum parametric output did not occur at the peak absorption of the NH_2D cell. The origin of the difficulty is that the microwave Stark cell was modified to prevent high voltage breakdown, thereby detuning its natural frequency from the original 4.134 GHz to nearly 3.8 GHz. Retuning to the desired frequency with an external tuning stub appears to be inefficient. Further investigation of other microwave Stark cells and the means for optimally coupling microwave radiation into it without disturbing the optical beam is in progress.

B. Microwave Stark Cell Development

During the course of the program radio frequency structures were developed for use in our modulation experiments. These devices included a modified version of our conventional Stark structure, a triplate resonator, and a ridged waveguide resonator.

The conventional Hughes Stark devices have 10 cm long gold-evaporated electrodes on alumina blocks spaced 1.2 mm apart. These blocks are enclosed in a steel can and the electrodes are fed by wires attached to two coaxial connectors. The alumina blocks provide excellent arc suppression to kilovolt potentials. Figure 7 shows the stainless steel can which encloses the alumina structure shown in the foreground. A triple stub matching transformer attached to the coaxial feed line was used to resonate the structure. A series of rf measurements determined that the device was not usable above 1 GHz because of spurious coupling between the feedlines and the can.

Several dummy and two operational triplate devices have been constructed. A unique feature of this design is that the microwave tuning structure and coupling probes are external to the vacuum cell, allowing continuous adjustment. However, severe rf radiation for the ends of the triplate structure into the laboratory was encountered above 200 MHz. While several shiedling techniques were employed to reduce the interference, in view of the very low level optical signals expected initially we decided to proceed with the completely enclosed ridged waveguide microwave structure.

A 20 cm long aluminum ridged waveguide resonator was constructed with a 5 mm wide ride and a 1.2 mm gap, shown in Fig. 8. The ridge was insulated from the rectangular structure by a thin layer of Teflon, allowing application of a dc Stark voltage to the ridge. The 4 GHz microwave energy is coupled into the device by means of a stub tuned probe.

Initial microwave measurements on the ridged waveguide structure showed the Q to be greater than 200. The tuning curve of the cavity is shown in Fig. 9. The device could be easily overcoupled

M10916

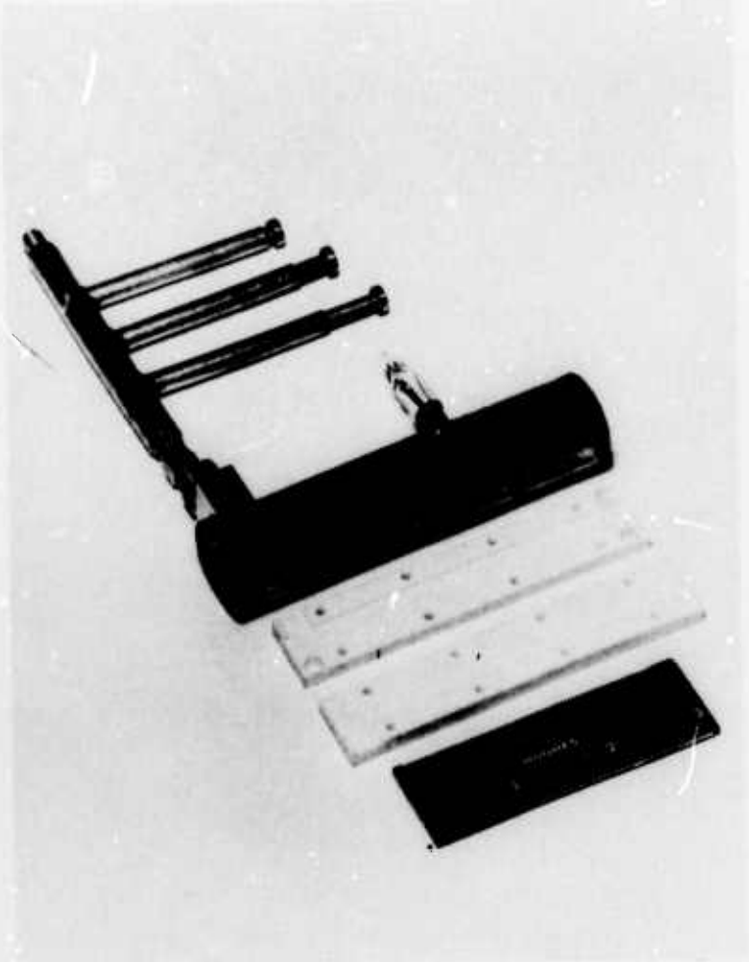

Fig. 7. Conventional Stark cell with 3 stub microwave tuning assembly attached. Alumina electrode structure shown in foreground.

M11293

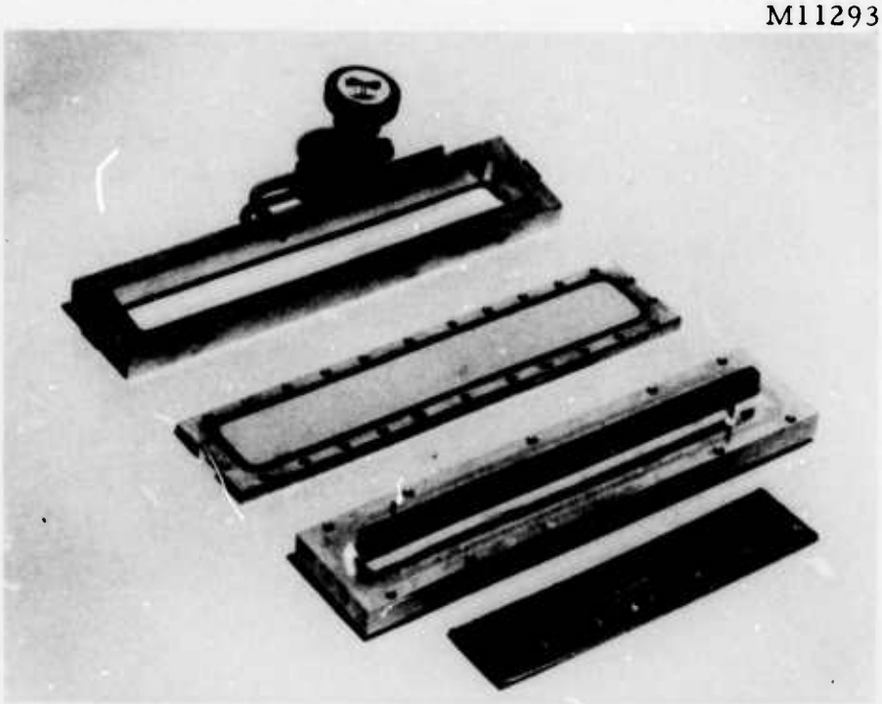

Fig. 8. Ridged waveguide NH_2D cavity. The ridge was insulated from the plate with Teflon and mylar sheets and attached with nylon screws. The leads for the HV bias, the microwave input and the microwave field probe are located beneath the lower plate.

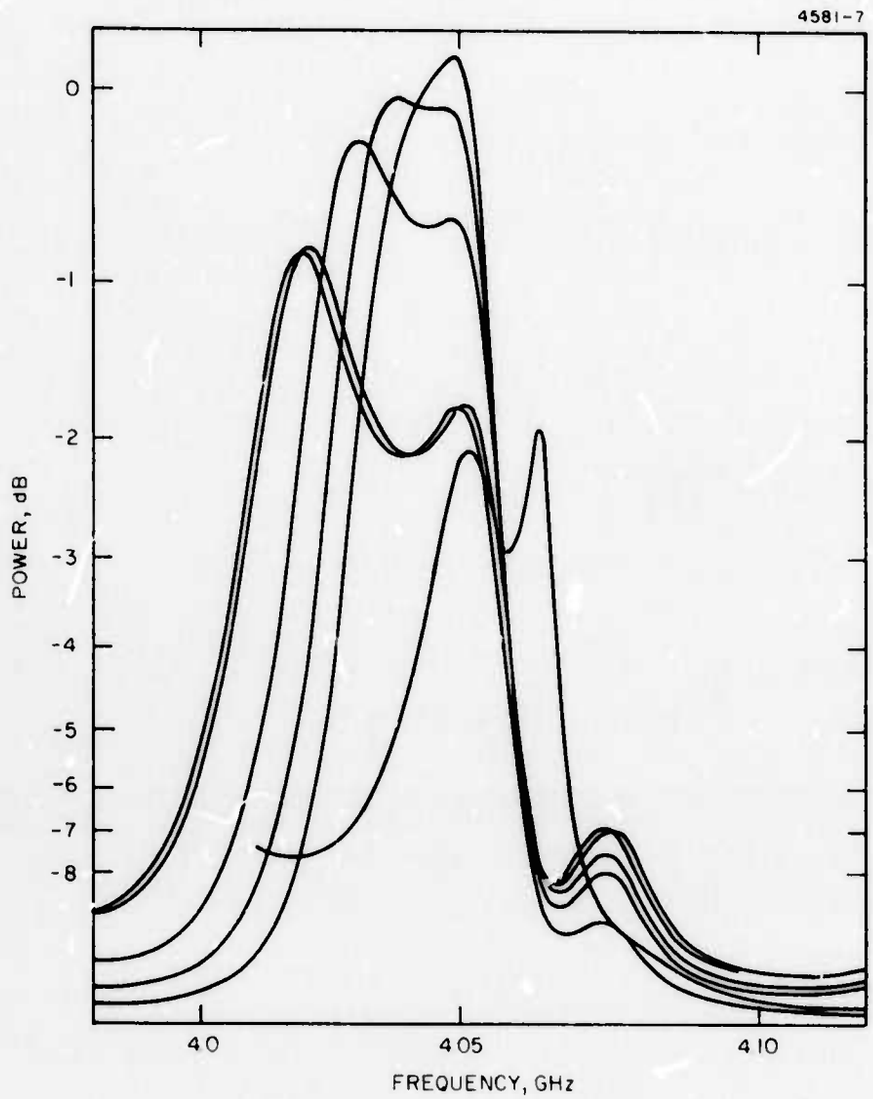

Fig. 9. Tuning curve for the ridged waveguide cavity. The ordinate is the microwave power coupled from the cavity with the probe. The abscissa is the frequency variation. By stub tuning the input, the probe input is readily changed, as shown.

as shown by the double-peaked resonances. Radiation leakage from the structure was found to be very small and easily manageable. The fields beneath the ridge were probed by pulling a lossy aquadag bead on a nylon string along the ridge and noting the regions of maximum microwave absorption. Five half-wavelength electric field peaks were measured along the structure at the 4.1 GHz frequency.

Intermittant arcing occurred initially in the ridge waveguide structure dissociating the NH_2D. Pachen breakdown near the ends of the ridge were found to be a problem area. The cavity was slightly modified; Teflon and epoxy coatings were applied to prevent the arcing. With extended bakeout processing, the cavity was finally made to withstand the voltages required for this experiment.

The characteristics of the modified cavity, however, were considerably changed from that of the original cavity. The cavity Q was reduced from 200 to 50; the resonance frequency was detuned for 4.13 GHz to about 3.8 GHz. In addition, the gap of the modified cavity was later found to be nonuniform, resulting in a peak NH_2D absorption of only 16% compared with 26% for the initial cavity. These changes from optimum did not prevent the first observation of the parametric oscillation in the NH_2D gas, but they did result in lower conversion efficiency than expected, the absence of saturation effects, and the detuning effects shown in Section III-E.

C. Experimental Apparatus for Observing Parametric Signal Output

The experimental apparatus for the observation of the interaction is discussed with reference to Fig. 10. A frequency stabilized CO_2 laser (operating at P(20) line center) is passed through the microwave Stark cell containing 1.1 Torr of NH_2D. The cell consists of a 4 GHz ridged waveguide cavity with a 5 mm wide ridge width, a 1.2 mm gap, and 20 cm length. The ridge is insulated from the rectangular structure by a thin layer of Teflon, allowing application of a dc Stark voltage to the ridge, as well as the 4 GHz microwave signal. The microwaves

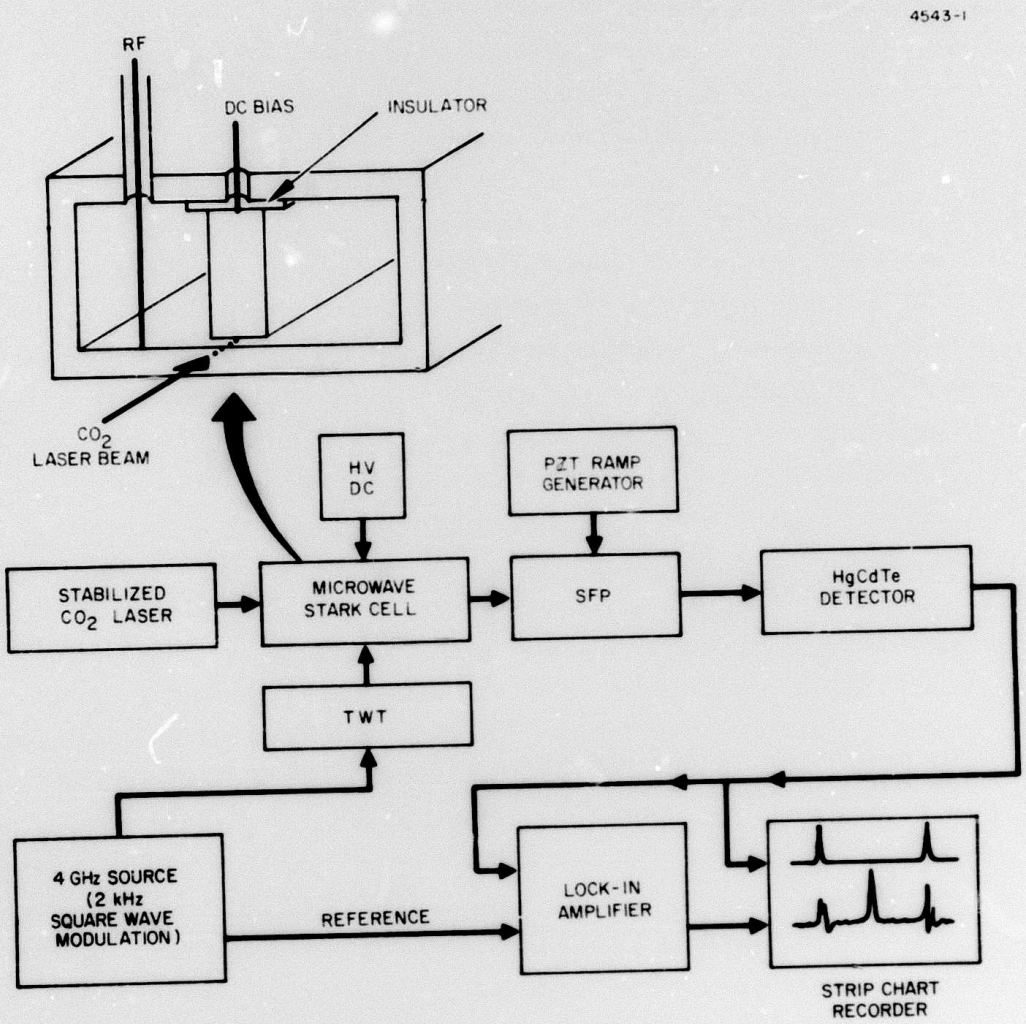

Fig. 10. Experimental apparatus for observation of single sideband signal. The traveling wave tube amplifier (TWT) supplies up to 16 W to the Stark cell, which is resonant at ~4.0 GHz.

are coupled into the cavity by means of a probe and the cavity is resonated at ~4 GHz with Q ~50. The resonant frequency can be adjusted by means of an external triple stub tuner. The microwaves are square wave amplitude modulated at ~2 kHz, amplified in a TWT to 16 W peak, and coupled into the microwave cavity.

The output of the Stark cell is passed through a Scanning Fabry-Perot interferometer (SFP) and detected with a HgCdTe photodiode. The SFP performs as a narrow bandwidth (300 MHz) optical filter that is slowly scanned through a 10 GHz free spectral range. The SFP output can then either be displayed directly on a recorder, or synchronously detected at the microwave modulation frequency in a lock-in amplifier. Very small changes in the SFP output due to the presence of the microwaves were detectable with the latter method. The initial measurements of the parametric signal were as described in Section III-D.

An x-y recorder was used in place of the strip recorder for the measurements of parametric signal versus Stark voltage, Stark cell pressure, and microwave power as described in Sections III E, F, G. The y-coordinate recorded the parametric signal, and the x-coordinate recorded the corresponding voltage, pressure and power. The SFP was not scanned but manually set to transmit only the parametric signal for these measurements.

The NH_2D was prepared by introducing equal partial pressures of NH_3 (from Matheson) and ND_3 (from ICN) in a mixing chamber. The resultant mixture containing 37.5% NH_2D was metered into the cell.

D. Observation of the Parametric Signal

The parametric signal resulting from the mixing of CO_2 laser light and 4 GHz microwave radiation in gaseous NH_2D contained in a microwave Stark cell was observed for the first time on 2 October 1975. The chart recording of a typical signal is described in this section.

Figure 11 shows the SFP output before and after lock-in detection; the two outputs are simultaneously displayed on a strip chart recorder as the SFP is slowly (100 sec) scanned through one full order. The upper trace shows the direct SFP signal, with the familiar pattern of a single mode laser. This is the SFP spectrum of 10.6 μm carrier transmitted through the cell to the detector. The free spectral range (FSR) is 10 GHz (1.5 cm plate spacing).

The lower trace of Fig. 11 shows the lock-in detection output. Signals occur at the positions corresponding to the peaks of the direct SFP output, indicating some sort of carrier modulation as a result of the applied microwave signal. A new peak, which is the parametric signal displaced 4 GHz from the carrier, appears approximately 40% of the way between the two carrier peaks. Note that only a single sideband occurs; double sideband generation would result in two signal peaks lying between the two carrier signals. Calibration of the SFP has verified that the sideband is a lower one, as predicted, and corresponds to the difference frequency between the 10.6 μm carrier frequency and the microwave frequency. That the output is a parametric signal and not fluorescence is substantiated by the fact that the sideband is linearly polarized and no other line is observed in the SFP output; if the output were fluorescence, unpolarized emission at several wavelengths would be expected.

The maximum parametric signal conversion efficiency (from the 10.6 μm carrier) was measured at $\sim 10^{-3}$ for the present cell compared with the theoretical value of 10^{-2}. Preliminary investigations indicate that inefficient microwave coupling, cavity detuning, and low cavity Q contribute to the lowered efficiency.

E. Parametric Signal as a Function of Stark Voltage and Microwave Frequency

The parametric signal was measured as a function of the Stark voltage for various microwave frequencies. The SFP sawtooth drive

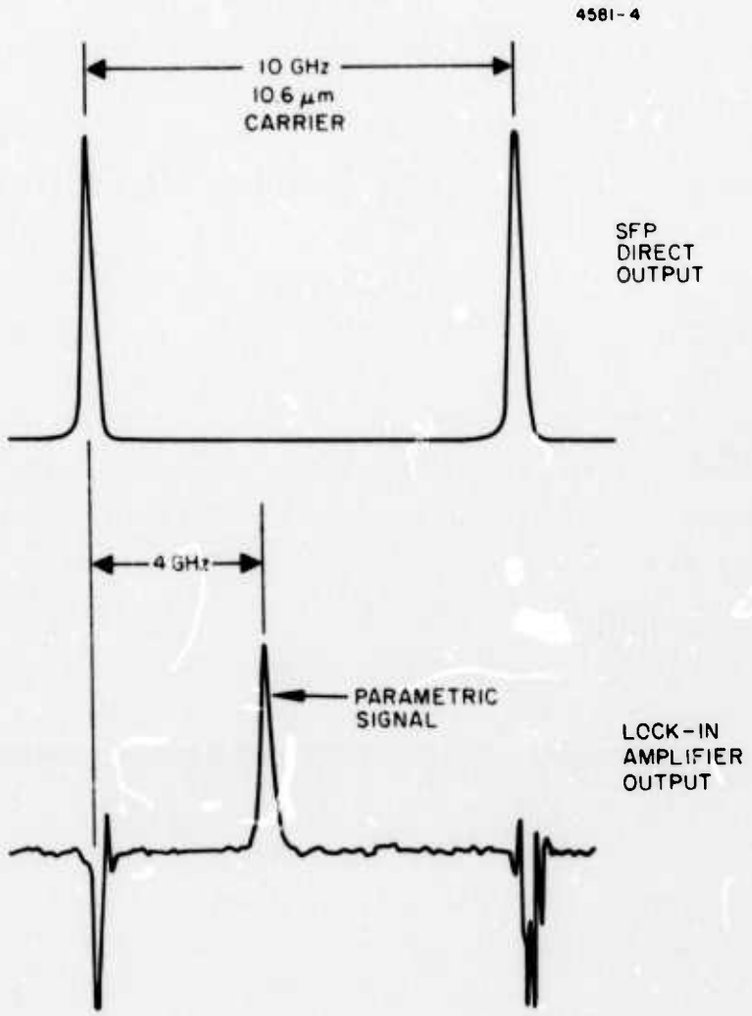

Fig. 11. Simultaneous signals observed.
(a) Directly from the detector.
(b) After phase sensitive detection as the SFP is scanned through one order. Note that the new feature due to the 4 GHz microwave signal appears as a single sideband 4 GHz away from the carrier.

was disconnected and the mirror spacing was set to transmit the peak of the parametric sideband signal for these measurements. The measured signal was displayed as the y-coordinate on an x-y recorder, with the x coordinate as the Stark voltage, for seven different microwave frequencies.

The maximum signal occurred at a Stark voltage of 428 V for the microwave frequency of 4.023 GHz, Fig. 12. The full width at half maximum (FWHM) of the signal was 27 V, which is equivalent to a linewidth of 122 MHz; the FWHM of the signal is essentially equal to the NH_2D linewidth at 1 Torr (80 MHz doppler width plus 30 MHz pressure broadening), as predicted by theory.

Figure 12 shows clearly that precise resonance interaction did not occur with the present modified Stark cell cavity. The maxima of the parametric signal at 4.023 GHz and the maxima of the absorption peak of the NH_2D gas (dotted line in Fig. 12), however, did not occur at the same Stark voltage. This implies that the 4.023 GHz frequency, though resulting the largest parametric signal, is not the central microwave resonance frequency. Indeed the positions of the peaks of the 4.104 GHz and the 4.150 GHz signals indicate that the central resonance frequency lies between these two frequencies, near the 4.134 GHz theoretically predicted. The natural resonant frequency of the microwave cavity, however, cannot be pulled this far without substantial loss of Q. During the next period a tunable waveguide CO_2 laser will be used to match resonances, thereby enhancing the parametric output.

A second signal peak arises at the Stark voltage of 575 V, as shown in Fig. 13. This corresponds to the parametric interaction with the $|M| = 3$ transitions.

F. Parametric Signal versus Stark Cell Pressure

The parametric signal was measured as a function of the Stark cell pressure over a range of 0 to 8 Torr. The SFP was set to transmit

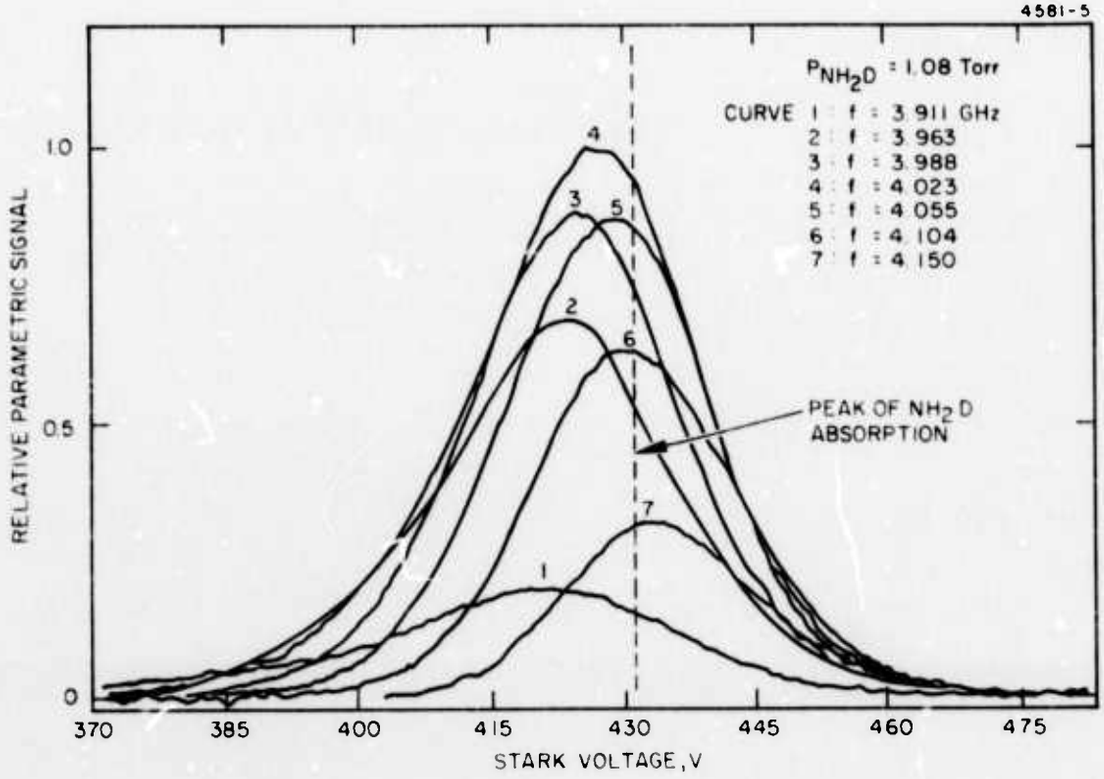

Fig. 12. Variation of parametric sideband signal with applied Stark voltage and microwave frequency. Note that the maximum parametric output did not occur at absorption peak.

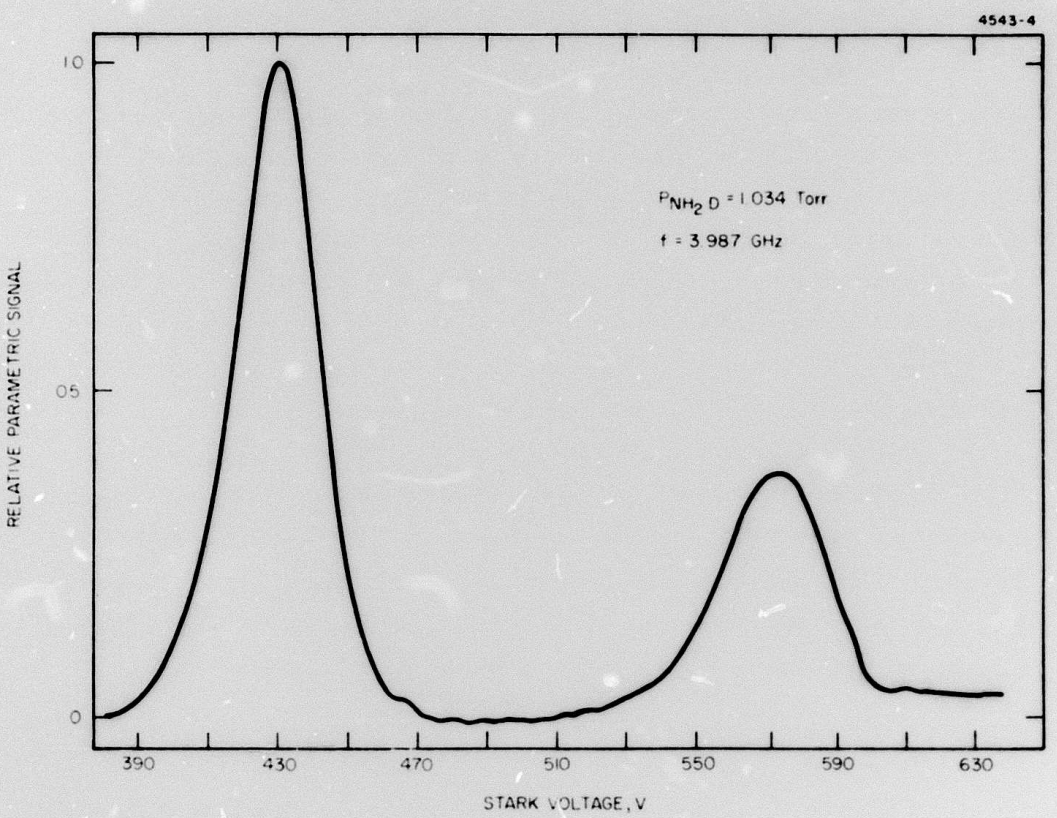

Fig. 13. Variation of parametric sideband signal with Stark voltage, showing interaction with $|M| = 4$ and $|M| = 3$ lines.

the maximum signal and the microwave frequency was fixed at 4.023 GHz. The parametric signal rose slowly between 0 and 0.5 (Fig. 14(a)), then rose sharply between 0.5 and 1.5 Torr, reaching a maximum at 2.4 Torr. The signal slowly decreased between 3 and 8 Torr (Fig. 14(b)).

The experimental curve of Fig. 14(b) and theory were compared; almost exact coincidence of the theoretical curve with the experimental curve was found. The signal varies as d^2 for small d values and small interaction distances (20 cm). The theoretical d values of Fig. 4 were squared and the abscissa was scaled so that the peak value of d^2 corresponded to the experimental peak of Fig. 14(a). The resulting theoretical points are shown in Fig. 14(b). The near coincidence of the theoretical points with the experimental curve is another factor affirming the theoretical description of the experiment.

The scaling of the abscissa was required to compensate for Stark field inhomogenities of the experimental cell. Subsequent to the experiments the Stark gap was remeasured and found to vary by 4% because of uneven insulator spacing under the ridge. The effect of the field inhomogenity was to broaden the resonance lines and to shift the signal maxima to higher pressures.

G. Parametric Signal Versus Microwave Power

The parametric signal output was found to be a linear function of the input microwave power. Figure 15 shows the linear relationship between parametric signal and microwave input power for the microwave source at 4.023 GHz and the Stark cell voltage set for the maximum parametric signal.

The linear relationship is expected for low microwave power. For the small value of x for our cell (20 cm) and for small values of g (0.01 cm^{-1}), the expression for η is approximately

$$\eta = \frac{g^2 x^2}{4} .$$

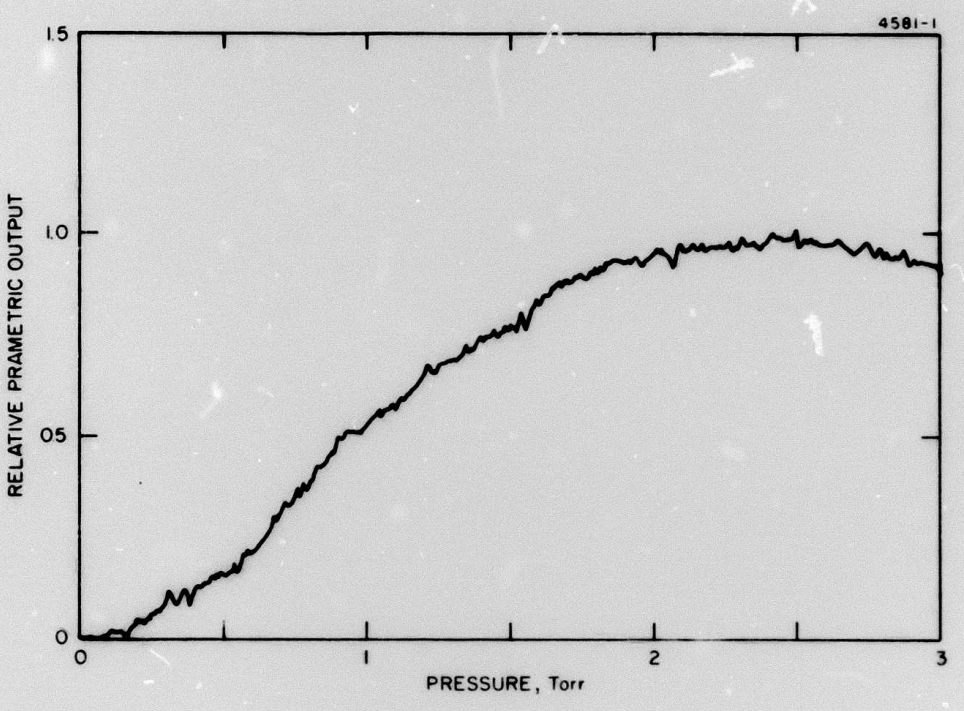

Fig. 14(a). Parametric signal versus low Stark cell pressure.

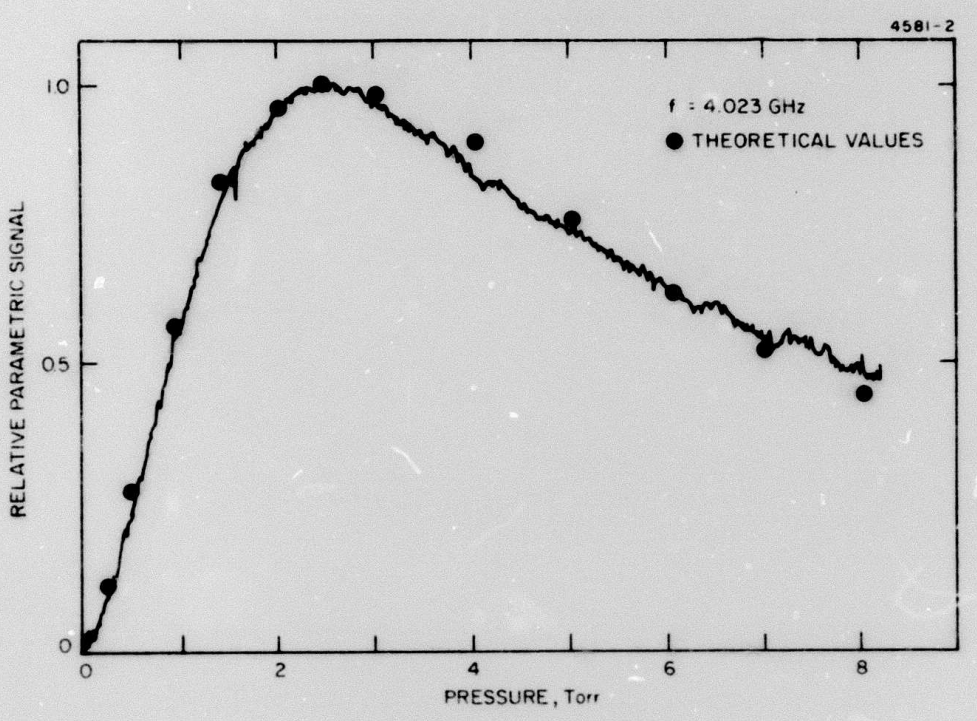

Fig. 14(b). Parametric signal versus Stark cell pressure 0 to 8 Torr.

Since g^2 is proportional to the microwave field power, η should vary as the microwave power for low powers.

For higher microwave powers, saturation effects are expected to saturate the parametric output, as calculated in Section II-G. Since Fig. 15 shows a linear relationship even for peak inputs of 16 W into the cavity, there is reason to believe that the microwave coupling into the ridge spacing of the present cavity is not efficient and that precise resonance matching conditions are not met. This is confirmed by the lower-than-expected conversion efficiency and the frequency pulling effect shown in Section III-E. Further investigation of the saturation effect will be made during the next period.

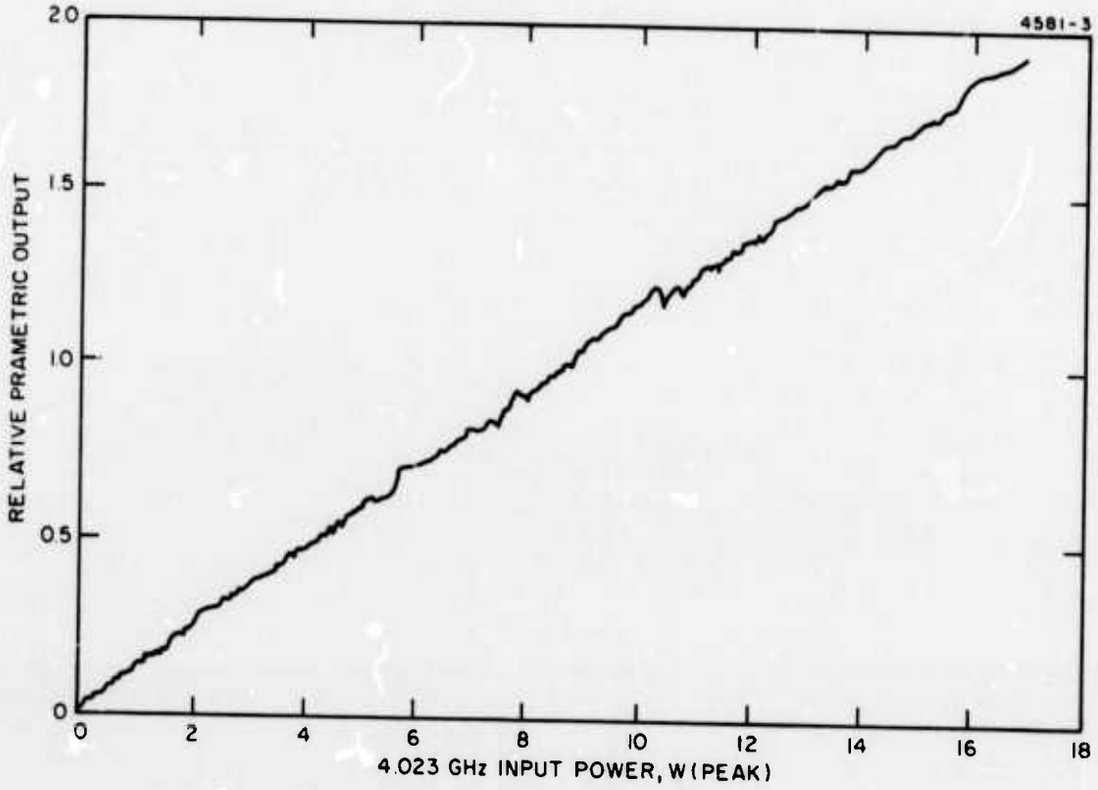

Fig. 15. Parametric signal versus microwave power.

REFERENCES

1. R. G. Brewer, M. J. Kelly, and A. Javan, Phys. Rev. Lett. 23, 559 (1969).

2. M. J. Kelly, R. E. Francke, and M. S. Feld, J. Chem. Phys. 53, 2979 (1970).

3. A. R. Johnston and R.D.S. Melville, Jr., Appl. Phys. Lett. 19, 503 (1971).

4. R. L. Abrams, Appl. Phys. Lett. 25, 304 (1974).

5. See, for example, N. Bloembergen, Nonlinear Optics (W. Benjamin, New York, 1962).

6. T. A. Nussmeier and R. L. Abrams, Appl. Phys. Lett. 25, 615 (1974).

7. A. Yariv, Introduction to Optical Electronics (Holt Rinehart and Winston, New York, 1972).

8. L. Thielman and L. W. Davis, Appl. Phys. Lett. 25, 461 (1974).